MOLECULAR AND CELLULAR BIOLOGY, Oct. 2011, p. 4176–4192 Vol. 31, No. 20
0270-7306/11/$12.00 doi:10.1128/MCB.05370-11

Deregulation of the p57-E2F1-p53 Axis Results in Nonobstructive Hydrocephalus and Cerebellar Malformation in Mice[▽]

Akinobu Matsumoto,[1,2] Etsuo Susaki,[1,2] Ichiro Onoyama,[1,2] Keiko Nakayama,[1,3] Mikio Hoshino,[4] and Keiichi I. Nakayama[1,2]*

Department of Molecular and Cellular Biology, Medical Institute of Bioregulation, Kyushu University, 3-1-1 Maidashi, Higashi-ku, Fukuoka, Fukuoka 812-8582, Japan[1]; CREST, Japan Science and Technology Agency (JST), Kawaguchi, Saitama 332-0012, Japan[2]; Department of Developmental Genetics, Center for Translational and Advanced Animal Research, Graduate School of Medicine, Tohoku University, 2-1 Seiryo-machi, Aoba-ku, Sendai 980-8575, Japan[3]; and Department of Biochemistry and Cellular Biology, National Institute of Neuroscience, National Center of Neurology and Psychiatry, Kodaira, Tokyo 187-8502, Japan[4]

Received 17 March 2011/Returned for modification 8 April 2011/Accepted 2 August 2011

The cyclin-dependent kinase inhibitor (CKI) p57^{Kip2} plays a pivotal role in cell cycle arrest during development, in particular, in the regulation of the entry of proliferating progenitors into quiescence. The gene encoding p57 undergoes genomic imprinting, and impairment of the regulation of p57 expression results in various developmental anomalies in humans and mice. We now show that p57 is expressed predominantly in the subcommissural organ and cerebellar interneurons in the mouse brain and that mice with brain-specific deletion of the p57 gene (*Kip2*) manifest prominent nonobstructive hydrocephalus as well as cerebellar malformation associated with the loss of Pax2-positive interneuron precursors and their descendants, including Golgi cells and γ-aminobutyric acid-containing neurons of the deep cerebellar nuclei. These abnormalities were found to be attributable to massive apoptosis of precursor cells in the developing brain. The morphological defects of the p57-deficient mice were corrected by knock-in of the gene for the related CKI p27^{Kip1} at the *Kip2* locus. The abnormalities were also prevented by additional genetic ablation of p53 or E2F1. Our results thus implicate p57 in cell cycle arrest in the subcommissural organ and Pax2-positive interneuron precursors, with the lack of p57 resulting in induction of p53-dependent apoptosis due to hyperactivation of E2F1.

Organogenesis can be viewed simplistically as the result of a combination of patterning cues acting on differentially proliferating tissues, and thus the shape of organs or tissues is intimately dependent on cell cycle control, in particular, on regulation of the exit of proliferating progenitors from the cell cycle. Cyclin-dependent kinase (CDK) inhibitors (CKIs) appear to play key roles in the timing of cell cycle exit before differentiation. For example, ablation of the CKI p27^{Kip1} in mice results in an increase in the number of granule cells in the cerebellum (21). The role of the CKI p57^{Kip2}, which is structurally related to p27, in such control of cell cycle exit remains poorly characterized, however, mainly because mice deficient in p57 die immediately after birth, manifesting severe developmental defects (33, 38, 40). We recently generated a knock-in mouse model (*Kip2*$^{[+]/Kip1KI}$) in which the nonimprinted allele of the p57 gene has been replaced with the mouse p27 gene (*Kip1*) (31). Most of the developmental defects characteristic of p57-deficient mice were corrected by p27 knock-in. Such observations highlight the importance of the control of cell cycle exit by CKIs for proper development.

The mammalian cerebellar cortex is a useful system for studies of the fundamental mechanisms controlling neurogenesis as a result of its relative simplicity, clear cytoarchitecture, and small number of neuronal cell types. Two primary regions of the embryonic brain, the rhombic lip and the ventricular zone of the embryonic fourth ventricle, give rise to the principal neurons that make up the cerebellum (1): the former region generates cerebellar granule cells and glutamatergic projection neurons of the deep cerebellar nuclei (DCN), whereas the latter produces Purkinje neurons and cerebellar interneurons, such as Golgi, stellate, and basket cells, as well as γ-aminobutyric acid (GABA)-containing interneurons of the DCN (3, 7). These various inhibitory interneurons are descendants of Pax2-positive precursors (15, 36).

The laminar structure of the cerebellum is composed of three main layers: the granule cell layer, Purkinje cell layer, and molecular layer (29). The localizations of cerebellar interneurons differ for the various cell types: stellate and basket interneurons reside in the molecular layer, whereas Golgi cells are present in the granule cell layer (30). Golgi, stellate, and basket cells are integral to cerebellar function as a result of their modulation of Purkinje and granule cell output, with the DCN serving as the main output centers of the cerebellum. However, little is known of the role of cell cycle regulation in the development of these cells.

We have now established mice in which the p57 gene is conditionally disrupted in the brain. Acute inactivation of p57 resulted in massive apoptosis predominantly in Pax2-positive

* Corresponding author. Mailing address: Department of Molecular and Cellular Biology, Medical Institute of Bioregulation, Kyushu University, 3-1-1 Maidashi, Higashi-ku, Fukuoka, Fukuoka 812-8582, Japan. Phone: 81-92-642-6815. Fax: 81-92-642-6819. E-mail: nakayak1@bioreg.kyushu-u.ac.jp.

▽ Published ahead of print on 15 August 2011.

interneuron precursors of the developing cerebellar primordium as well as in severe nonobstructive hydrocephalus. Our observations indicate that p57 regulates the activities of E2F1 and p53 to ensure the proper proliferation and survival of cells in the subcommissural organ (SCO) as well as of Pax2-positive cells in the cerebellar primordium.

MATERIALS AND METHODS

Antibodies. Antibodies to p57 for immunofluorescence analysis (M-20, H-91) or for immunoblot analysis were obtained from Santa Cruz Biotechnology (Santa Cruz, CA) and Sigma (St. Louis, MO), respectively; those to calbindin or parvalbumin were from Swant (Bellinzona, Switzerland); those to GABA or βIII-tubulin were from Sigma; those to neurogranin or NeuN were from Millipore (Schwalback, Germany); those to bromodeoxyuridine (BrdU), p27, or HSP90 were from BD Biosciences (San Diego, CA); those to nestin or Lhx1/5 were from Developmental Studies Hybridoma Bank (Iowa City, IA); those to glial fibrillary acidic protein (GFAP), myelin basic protein (MBP), Pax2, activated caspase-3, or SMI32 were from DakoCytomation (Riga, Latvia), Abcam (Cambridge, United Kingdom), Zymed (San Francisco, CA), Cell Signaling (Danvers, MA), and Calbiochem (San Diego, CA), respectively; those to Rb or Ser^{780}-phosphorylated Rb were from Cell Signaling Technology; those to Ptf1a were generated in-house (8); and those to Corl2 were kindly provided by Y. Ono.

Generation of nestin-Cre/*Kip2*$^{[+]/F}$ mice. The generation of *Kip2*$^{[+]/F}$ mice was described elsewhere (16). Briefly, the 5′ and 3′ regions of homology in the targeting vector for the p57 gene (*Kip2*) were generated by PCR with appropriate primers. The neomycin resistance gene (*neo*) flanked by *loxP* sites was isolated from the plasmid pL2-Neo (kindly provided by D. R. Littman) and inserted downstream of exon 4 of *Kip2*, and a *loxP* site was also inserted upstream of exon 2. A diphtheria toxin A cassette was ligated at the 5′ end of the targeting construct. The maintenance, transfection, and selection of embryonic stem (ES) cells were performed as previously described (23, 24). The recombination event was confirmed by Southern blot analysis. ES clones that had undergone homologous recombination were transfected with pMC-Cre (kindly provided by D. R. Littman) to excise the *loxP-neo* cassette. Colonies were screened for acquired sensitivity to G418, and loss of the cassette was confirmed by Southern blot analysis. ES clones were injected into C57BL/6 mouse blastocysts to generate chimeric mice, and germ line transmission of the floxed *Kip2* allele was achieved by crossing chimeras with C57BL/6 mice. Female mice heterozygous for the floxed *Kip2* allele (*Kip2*$^{[+]/F}$ or *Kip2*$^{[F]/+}$; symbols within brackets represent the imprinted, inactive allele) were then crossed with male nestin-Cre transgenic mice (34) to generate nestin-Cre/*Kip2*$^{[+]/F}$ offspring. Deletion of *Kip2* in these offspring was detected by PCR analysis with the primers AM83 (5′-ATGAGC GTCTGTTAGGGACAGAC-3′), AM84 (5′-GACCAGACAGTCGAAATGGT TCC-3′), and AM85 (5′-GCCGCGGTGTTGTTGAAACTG-3′).

Other mice. Nestin-Cre/*Kip2*$^{[+]/F}$ mice were also crossed with *Tp53*$^{-/-}$ mice (Taconic, Hudson, NY), *Kip1*$^{-/-}$ mice (23), or *E2f1*$^{-/-}$ mice (37). *Kip2*$^{[+]/Kip1KI}$ mice were described previously (31). All mouse experiments were approved by the animal ethics committee of Kyushu University.

Immunoblot analysis. Total protein extracts were prepared from tissue with the use of radioimmunoprecipitation assay buffer and were subjected to immunoblot analysis as previously described (31).

Quantitative RT-PCR analysis. Total RNA was extracted from tissue by the guanidinium thiocyanate-phenol-chloroform method, purified, and subjected (1 μg) to reverse transcription (RT) with random hexanucleotide primers (QuantiTect RT kit; Qiagen, Tokyo, Japan). The resulting cDNA was then subjected to real-time PCR analysis with 1× SYBR green PCR master mix (TaKaRa, Shiga, Japan) and 200 nM gene-specific primers. Assays were performed in triplicate with a StepOnePlus real-time PCR system (Applied Biosystems, Foster City, CA). The amplification protocol comprised initial incubation at 60°C for 30 s and 95°C for 3 s, followed by 40 cycles. The sequences of the various primers (sense and antisense, respectively) were 5′-GGACCCGAGAAGACCTCCTT-3′ and 5′-GCACATCACTCAGAATTTCAATGG-3′ for hypoxanthine phosphoribosyltransferase (HPRT), 5′-TGTCTTGCACTCTGGTGTCTGAGC-3′ and 5′-TCTTGCAGAAGACCAATCTGCG-3′ for p21, 5′-AGTGTCCAGGGATGAG GAAGCGAC-3′ and 5′-TTCTTGGGCGTCTGCTCCACAGTG-3′ for p27, 5′-GCGCAAACGTCTGAGATGAGT-3′ and 5′-AGAGTTCTTCCATCGTCCG CT-3′ for p57, 5′-ACTCAGGAAGATCGGAGACAAAGTG-3′ and 5′-ACAC TCGTCCTTCAAGTCTGCTGG-3′ for Noxa, 5′-CGCAGGAAGAATGAAAA GAGGG-3′ and 5′-CTGAGGAAGCAGGAAGTGAGAGTC-3′ for Mcm3, 5′-AGTTCTGTGCCCGCAAAGTG-3′ and 5′-AGCAGCAAAGAGCAAACCA GG-3′ for Cdc6, 5′-TATGGAGGTGGTCTGTGCAA-3′ and 5′-GGCAAGGA GCTCAAAGTCAC-3′ for Cdt1, and 5′-ACCTGCAGAACCTTACCATCG A-3′ and 5′-AGTCATGGCTCTGCTTCAGGTC-3′ for p73. Reactions for HPRT mRNA were performed concurrently on the same plate as those for the test mRNAs, and results were normalized by the corresponding amount of HPRT mRNA.

Histological and immunohistofluorescence analysis. Tissue was fixed with 4% paraformaldehyde in phosphate-buffered saline (PBS). For hematoxylin-eosin staining, the fixed tissue was embedded in paraffin and cut into serial sections with a thickness of 4 μm. For immunofluorescence staining, the fixed tissue was cut serially into 40-μm-thick sections with a vibrating microtome (VT1000; Leica, Wetzlar, Germany). The sections were then incubated for 2 days at room temperature with primary antibodies in PBS containing 1% bovine serum albumin and 0.3% Triton X-100, washed thoroughly with PBS, and incubated overnight at room temperature with Alexa Fluor 488- or Alexa Fluor 546-conjugated goat secondary antibodies (Molecular Probes, Eugene, OR). Cell nuclei were stained with Hoechst 33258. The sections were finally mounted with Vectashield medium (Vector, Burlingame, CA) and examined with a laser-scanning confocal microscope (LSM510; Carl Zeiss, Oberkochen, Germany). For BrdU labeling, dams were injected intraperitoneally with BrdU (40 μg per gram of body weight; BD Biosciences) before immunostaining of isolated embryos.

Primary culture. Neurons were isolated from the cerebella of mice at postnatal day 0.5 (P0.5) and were cultured with the use of a nerve cell culture system (Sumitomo, Tokyo, Japan) in dishes coated with poly-L-lysine (Sigma). After being cultured for 7 days, the cells were fixed with 4% paraformaldehyde and incubated with antibodies to p57, βIII-tubulin, GFAP, or MBP. Immune complexes were detected with Alexa Fluor 488- or Alexa Fluor 546-conjugated goat secondary antibodies (Molecular Probes). Cell nuclei were stained with Hoechst 33258.

Statistical analysis. Quantitative data are presented as means ± standard deviations (SD) and were analyzed by Student's *t* test. A P value of <0.05 was considered statistically significant.

RESULTS

p57 is expressed predominantly in the SCO and Pax2-positive neurons. We examined the expression of p57 in the brains of wild-type mice and found that only a small subset of cerebellar cells expressed this CKI during early postnatal development. Most cerebellar cells reactive with antibodies to Pax2, a marker of inhibitory interneuron precursors (15, 36), also expressed p57 (Fig. 1A). We confirmed that only a small subset of neurons—not astrocytes or oligodendrocytes—expressed p57 in primary cultured cells isolated from neonatal cerebella (Fig. 1B). We measured the percentages of p57-positive cells among neurons (βIII-tubulin$^+$), astrocytes (GFAP$^+$), and oligodendrocytes (MBP$^+$) after 2 and 7 days of primary culture (Fig. 1C). After 2 days of culture, >15% of neurons were positive for p57, whereas <5% of neurons were positive for p57 after 7 days. We did not detect p57 expression in GFAP- or MBP-positive cells at any time point examined. Given that the number of neurons did not change substantially during culture (data not shown), these results suggested that p57 is specifically expressed in neural precursor cells of the cerebellum and that these cells lose p57 expression during differentiation in culture. This downregulation of p57 expression during culture may recapitulate that which normally occurs in the mouse cerebellum after birth (Fig. 1A). The number of p57-expressing cells thus decreased after birth as the cells differentiated, and they were almost undetectable at P15 (data not shown). These patterns of p57 expression in the developing cerebellum suggested that p57 functions to restrain the cell cycle when immature Pax2-positive interneuron precursors begin to differentiate and to cease proliferating. In addition, p57 was found to be highly expressed in the SCO, especially around the lateral region, at embryonic day 14.5 (E14.5) (Fig. 1D).

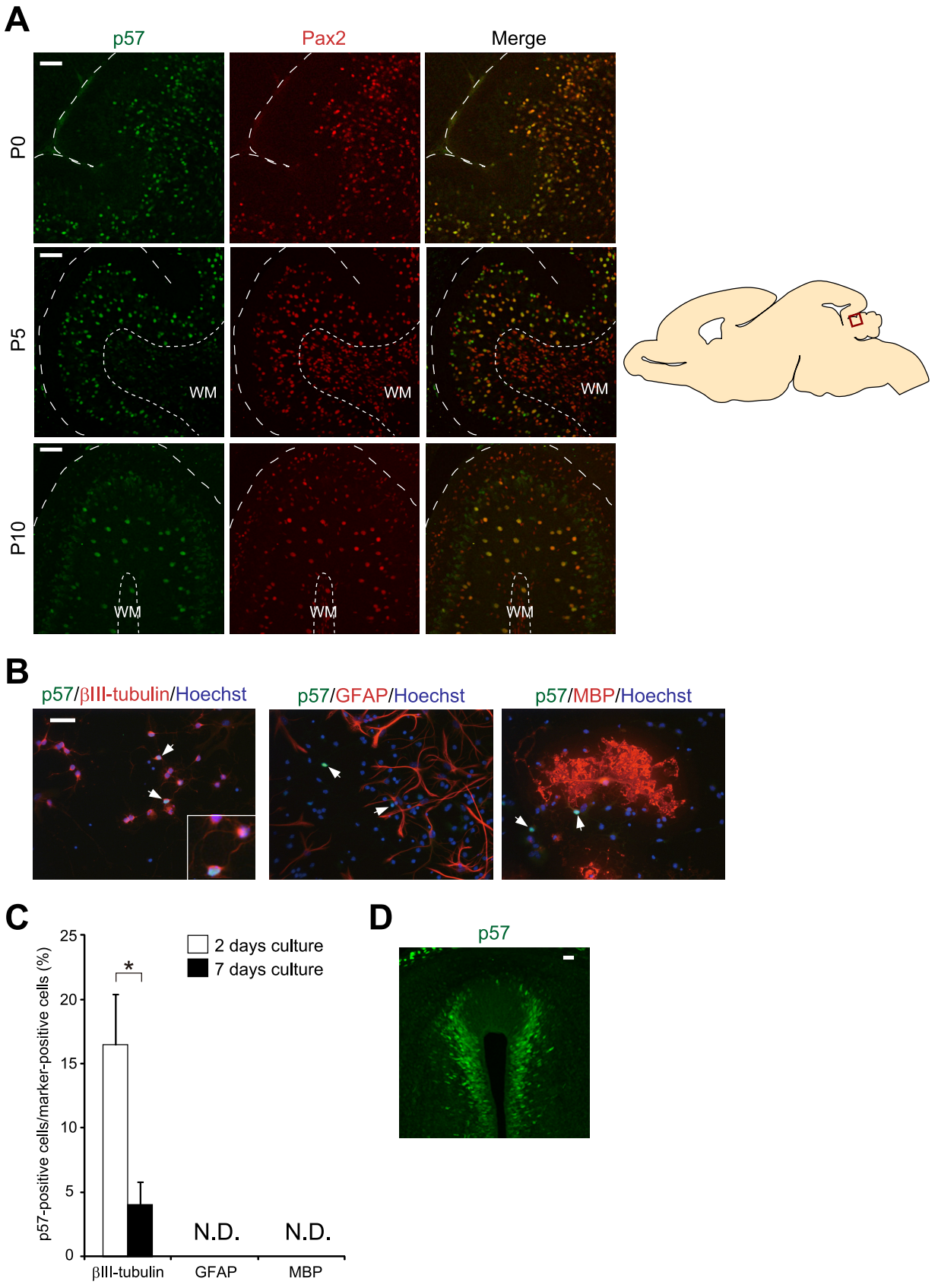
A
p57
Pax2
Merge
P0
P5
P10
WM
B
p57/βIII-tubulin/Hoechst
p57/GFAP/Hoechst
p57/MBP/Hoechst
C
2 days culture
7 days culture
p57-positive cells/marker-positive cells (%)
25
20
15
10
5
0
*
N.D.
N.D.
βIII-tubulin
GFAP
MBP
D
p57

p57 deficiency in the brain leads to severe hydrocephalus. The *Kip2* locus undergoes genomic imprinting, with only the maternal allele being expressed (17). To ablate the maternal *Kip2* allele only in the nervous system, we crossed female mice heterozygous for the floxed allele (*Kip2*$^{[F]/+}$ or *Kip2*$^{[+]/F}$; symbols within brackets represent the imprinted, inactive allele) (17) with male mice harboring a *Cre* transgene under the control of the promoter for the nestin gene, to yield nestin-Cre/*Kip2*$^{[+]/F}$ mice. We confirmed that the floxed allele was efficiently inactivated by Cre in the brain of the resulting offspring, although a small subset of cells retained the floxed allele (Fig. 2A to C).

Whereas most conventional p57 knockout (*Kip2*$^{[+]/-}$) mice die soon after birth as a result of respiratory distress likely caused by skeletal anomalies, nestin-Cre/*Kip2*$^{[+]/F}$ mice were born in approximately the expected Mendelian ratio. The developmental defects of the palate and intestine apparent with conventional p57 knockout mice were absent in nestin-Cre/*Kip2*$^{[+]/F}$ mice (data not shown). In contrast, like conventional p57 knockout mice, nestin-Cre/*Kip2*$^{[+]/F}$ mice exhibited abnormal lens development at E16.5 (Fig. 2D). The body size of the mutant mice was substantially smaller than that of wild-type littermates, and skeletal deformities, such as protrusion of the skull and kyphosis, were apparent in the nestin-Cre/*Kip2*$^{[+]/F}$ animals (Fig. 2E and F). The mutant mice also showed a balance disorder and ataxic gait (data not shown). Nestin-Cre/*Kip2*$^{[+]/F}$ mice died as early as 2 weeks of age, with most dying within 3 weeks after birth (Fig. 2G). Histopathologic examination revealed severe hydrocephalus in mutant brains at P15 (Fig. 2H), although no apparent anatomic obstruction was detected (a condition known as communicating or nonobstructive hydrocephalus). The ventricles were greatly expanded, and the cerebral cortex exhibited marked thinning at P15 as a result of hydrocephalus. One of the causes of nonobstructive hydrocephalus is damage to the SCO, which synthesizes SCO-spondin, a component of Reissner's fiber, which is required for the smooth flow of cerebrospinal fluid (18). As mentioned above, p57 is highly expressed in the lateral region of the SCO at E14.5 (Fig. 1D). In nestin-Cre/*Kip2*$^{[+]/F}$ mice, the SCO at P5 appeared atrophic, with ependymal denudation (Fig. 2I). We found that p57 was efficiently ablated in the SCO region at E14.5 (Fig. 2J). These results suggested that dysfunction of the SCO is responsible for the nonobstructive hydrocephalus of the mutant mice. The thinning of the cerebral cortex in nestin-Cre/*Kip2*$^{[+]/F}$ mice apparent at P15 was likely a secondary effect of the hydrocephalus attributable to the SCO defect. No impairment of layer formation in the cerebral cortex was apparent in nestin-Cre/*Kip2*$^{[+]/F}$ mice at E18.5, which is before the onset of hydrocephalus (Fig. 2K).

Malformation of and loss of Pax2-positive cells in the p57-deficient cerebellum. Gross inspection revealed the cerebellum of nestin-Cre/*Kip2*$^{[+]/F}$ mice to be atrophic and deformed (Fig. 3A). Histopathologic examination showed that the normal layered structure of the cerebellum—consisting of the granule cell, Purkinje cell, and molecular layers—was highly defective in the mutant mice (Fig. 3A and B). We also examined sagittal sections of the cerebella from nestin-Cre/*Kip2*$^{[+]/+}$ and nestin-Cre/*Kip2*$^{[+]/F}$ mice at P15 (Fig. 3C). Cerebellar malformation in nestin-Cre/*Kip2*$^{[+]/F}$ mice was apparent only in the hemispheres, not in the vermis. The morphological deformity was most profound in the anterior region of the cerebellar hemispheres of nestin-Cre/*Kip2*$^{[+]/F}$ mice. However, the size of and folium number for all regions of the cerebellum were substantially smaller for nestin-Cre/*Kip2*$^{[+]/F}$ mice than for control mice. The differences in the extent of malformation are likely attributable to those in the efficiency of *Kip2* deletion by Cre, whose expression is driven by the nestin gene promoter. The efficiency of *Kip2* deletion by Cre recombinase in nestin-Cre/*Kip2*$^{[+]/F}$ mice was relatively low (Fig. 2A to C). By means of immunostaining for p57, we examined the deletion efficiency for *Kip2* in various regions of the cerebella of nestin-Cre/*Kip2*$^{[+]/F}$ mice at P0.5 (Fig. 3D and E). Cells reactive with antibodies to p57 were virtually absent (that is, *Kip2* was almost completely deleted) in the anterior region of the cerebellar hemispheres in nestin-Cre/*Kip2*$^{[+]/F}$ mice, whereas p57 was still expressed in ~40% of cells (unlike in control mice) in the posterior region of the hemispheres. On the other hand, p57 expression in the vermis of the cerebella (both anterior and posterior regions) of nestin-Cre/*Kip2*$^{[+]/F}$ mice did not differ significantly from that in control mice. These results indicate that the extent of malformation in the cerebellum is well correlated with the extent of *Kip2* deletion. We thus conclude that the loss of p57 results in a marked defect in the normal development of the cerebellum.

We next performed immunofluorescence analysis with antibodies to calbindin as a marker for Purkinje cells, to GFAP as a marker for astrocytes, and to MBP as a marker for oligodendrocytes. Purkinje cells were present but were highly disorganized in the cerebella of nestin-Cre/*Kip2*$^{[+]/F}$ mice (Fig. 4A). In addition to neurons, glial cells, such as astrocytes and oligodendrocytes, appeared atrophic and unorganized (Fig. 4A). Given that hydrocephalus in other mutant mouse models is not usually accompanied by cerebellar anomalies (5, 10, 28), the disorganized layer pattern in the cerebella of nestin-Cre/*Kip2*$^{[+]/F}$ mice is not likely a secondary effect of hydrocephalus. These results thus suggested that the loss of p57 affects the morphology of most cells in the cerebellum, resulting in severe cerebellar malformation.

FIG. 1. Expression of p57 in Pax2-positive cells in the cerebellum. (A) Immunofluorescence staining of Pax2 and p57 in the cerebellum (demarcated by the dashed line) of a wild-type mouse at P0, P5, and P10. WM, white matter. Scale bar, 50 μm. A schematic representation of the brain is also shown, with the red box indicating the position of the section. (B) Primary cultures prepared from the cerebella of wild-type mice at P0.5 and maintained for 7 days were subjected to immunofluorescence analysis of p57, βIII-tubulin, GFAP, and MBP, as indicated. Cell nuclei were stained with Hoechst 33258. Arrows indicate p57-positive cells. βIII-Tubulin staining is shown at higher magnification in the inset, revealing the cytoplasmic localization of this protein. Scale bar, 40 μm. (C) Quantitative analysis of cells positive for p57 among the various marker-positive cells in primary cultures prepared from the cerebella of wild-type mice at P0.5 and maintained for 2 or 7 days. Data are means ± SD ($n = 3$). *, $P < 0.003$; N.D., not detected. (D) Immunofluorescence staining of p57 in the SCO of a wild-type mouse at E14.5. Scale bar, 25 μm.

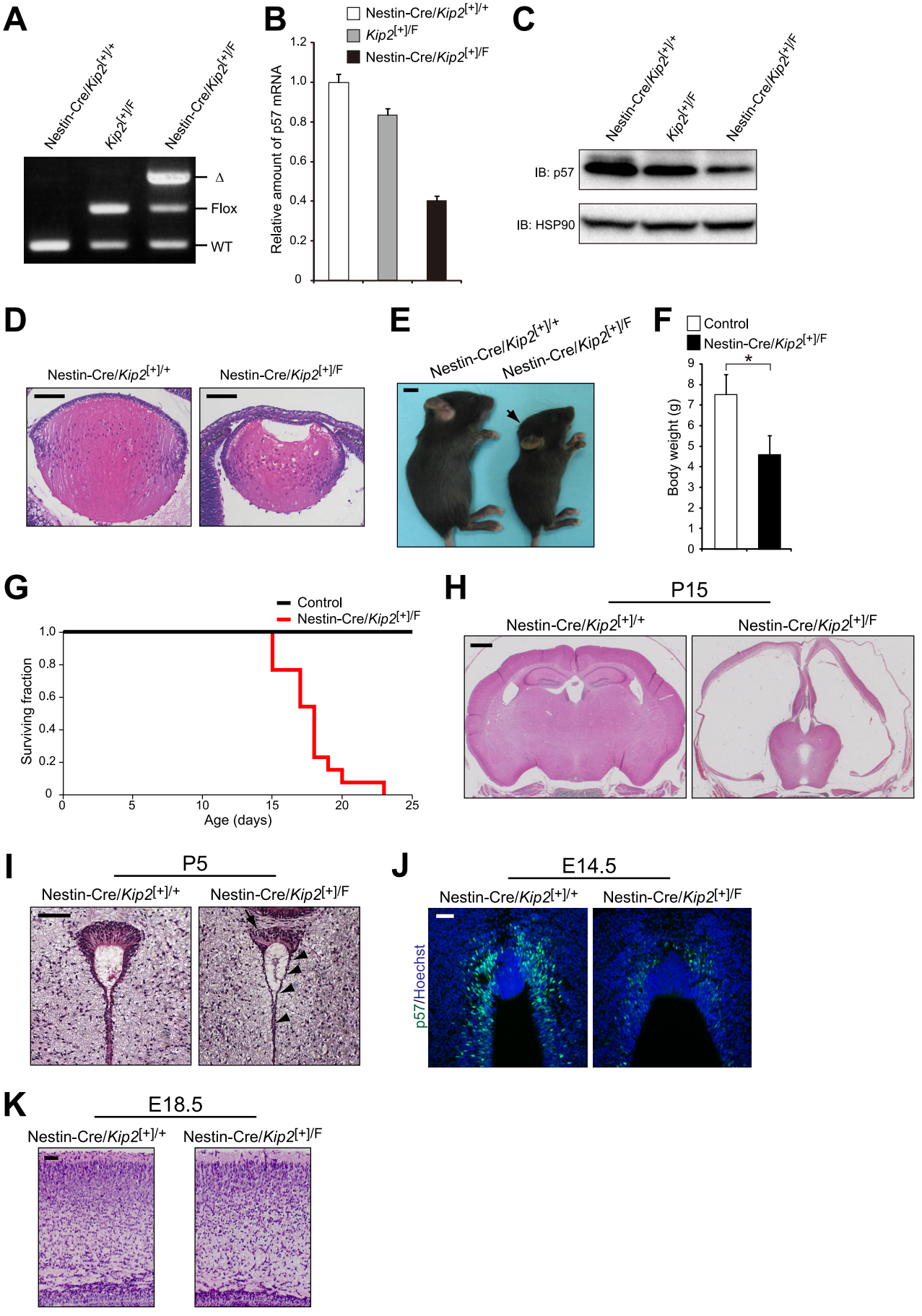
A
Nestin-Cre/Kip2[+]/+
Kip2[+]/F
Nestin-Cre/Kip2[+]/F
Δ
Flox
WT
B
Nestin-Cre/Kip2[+]/+
Kip2[+]/F
Nestin-Cre/Kip2[+]/F
Relative amount of p57 mRNA
1.2
1.0
0.8
0.6
0.4
0.2
0
C
Nestin-Cre/Kip2[+]/+
Kip2[+]/F
Nestin-Cre/Kip2[+]/F
IB: p57
IB: HSP90
D
Nestin-Cre/Kip2[+]/+
Nestin-Cre/Kip2[+]/F
E
Nestin-Cre/Kip2[+]/+
Nestin-Cre/Kip2[+]/F
F
Control
Nestin-Cre/Kip2[+]/F
*
Body weight (g)
9
8
7
6
5
4
3
2
1
0
G
Control
Nestin-Cre/Kip2[+]/F
Surviving fraction
1.0
0.8
0.6
0.4
0.2
0
0
5
10
15
20
25
Age (days)
H
P15
Nestin-Cre/Kip2[+]/+
Nestin-Cre/Kip2[+]/F
I
P5
Nestin-Cre/Kip2[+]/+
Nestin-Cre/Kip2[+]/F
J
E14.5
Nestin-Cre/Kip2[+]/+
Nestin-Cre/Kip2[+]/F
p57/Hoechst
K
E18.5
Nestin-Cre/Kip2[+]/+
Nestin-Cre/Kip2[+]/F

Despite the fact that various cell types in the cerebellum were affected by the loss of p57, p57 is expressed predominantly in Pax2-positive cells (Fig. 1A). We therefore examined the number and development of Pax2-positive cells in the cerebella of nestin-Cre/*Kip2*$^{[+]/F}$ mice. The number of Pax2-positive cells was greatly reduced in the cerebella of nestin-Cre/*Kip2*$^{[+]/F}$ mice at P0 (Fig. 4B). Although a small number of Pax2-positive cells remained in the mutant cerebellum, these cells also expressed p57 (Fig. 4C), indicating that deletion of the floxed *Kip2* allele was not complete. Pax2-positive cells yield GABA-positive DCN, Golgi, stellate, and basket cells within 2 weeks after a mouse's birth (15, 36). Among these cell populations, GABA-positive DCN and neurogranin-positive Golgi cells were virtually absent in nestin-Cre/*Kip2*$^{[+]/F}$ mice at P15 (Fig. 4D). In contrast, stellate and basket cells, both of which are recognized as parvalbumin-positive and calbindin-negative cells in the molecular layer, were present in nestin-Cre/*Kip2*$^{[+]/F}$ mice, although their arrangement was markedly disorganized. These results suggested that the Pax2-positive cells remaining as a result of incomplete deletion of *Kip2* specifically yielded stellate and basket cells or that the lineage of stellate and basket cells neither expresses p57 nor depends on p57 for survival. The number of and the area occupied by SMI32-positive glutamatergic DCN neurons (8) were also markedly decreased in nestin-Cre/*Kip2*$^{[+]/F}$ mice (Fig. 4D). Together, our observations thus suggested that ablation of p57 results in the loss of GABA-positive DCN and Golgi cells, a subset of the descendants of Pax2-positive cells, and that this loss gives rise to the disorganized layers of the cerebellum.

p57 deficiency results in apoptosis during embryonic development. To explore the mechanism underlying the decrease in the number of Pax2-positive interneuron precursors in nestin-Cre/*Kip2*$^{[+]/F}$ mice, we examined whether such cells might be eliminated by apoptosis during development. Immunostaining for the cleaved (activated) form of caspase-3 revealed that the level of apoptosis was greatly increased in the cerebellar primordia of nestin-Cre/*Kip2*$^{[+]/F}$ mice at E12.5 compared with that in control mice (Fig. 5A). The frequency of apoptosis in the mutant embryos was reduced at E14.5 and E16.5 compared with that at E12.5, but it was still greater than that in age-matched control animals (Fig. 5B to D). In addition, an increased level of apoptosis was apparent in the SCO region of nestin-Cre/*Kip2*$^{[+]/F}$ mice compared with that of control animals (Fig. 5E). These results thus suggested that the loss of Pax2-positive cells and defects of the SCO in the mutant mice are attributable to an increased level of apoptosis resulting from p57 deficiency.

At E12.5, however, only a small number of p57-positive cells in the cerebellar primordia of wild-type mice also expressed Pax2, whereas the number of such cells was increased at E14.5 (Fig. 6A and B). In the cells expressing both p57 and Pax2, the level of p57 expression varied at E12.5, probably reflecting cell cycle status. Most cells that expressed p57 were also positive for Pax2 at E14.5 and E16.5. Given that p57 is abundant in many cells other than Pax2-positive cells in this region at E12.5, we attempted to characterize the p57-positive cells by combined immunostaining with antibodies to nestin (a marker for neural progenitor cells), to NeuN (a marker for mature neurons), to βIII-tubulin (a marker for mature neurons), to Ptf1a (a marker for progenitors of all GABAergic neurons [8]), to Lhx1/5 (a marker for GABAergic neurons, including GABA-positive DCN neurons, Purkinje cells, and inhibitory interneurons [3]), or to Corl2 (a marker for immature Purkinje cells [20]). Most p57-positive cells were not reactive with antibodies to nestin or to βIII-tubulin (Fig. 6C and D), suggesting that p57 is expressed transiently in neuronal cells at a stage intermediate between the nestin-positive and βIII-tubulin/NeuN-positive stages. The expression of p57 overlapped partially that of Ptf1a (Fig. 6C and D), but it persisted longer than did that of Ptf1a. In contrast, the expression of p57 also overlapped partially that of Lhx1/5 (Fig. 6C and D), but it appeared earlier than did that of Lhx1/5. *In vivo* labeling with BrdU revealed that the cells expressing p57 at E12.5 incorporated BrdU when it was administered to pregnant females at E11.9 (Fig. 6E), suggesting that the p57-positive cells were generated from neural progenitor cells at E11.9. Cells generated from neural progenitors at this stage were previously shown to be either Purkinje cells, Golgi cells, or glutamatergic DCN neurons (19). However, the expression of p57 did not overlap substantially that of Corl2 (Fig. 6C and D), making it unlikely that the p57-positive cells are immature Purkinje cells. These findings, together with our observation that Golgi cells and GABAergic DCN neurons were virtually absent in nestin-Cre/*Kip2*$^{[+]/F}$ mice (Fig. 4D), suggested that most of the cells expressing p57 at E12.5 might differentiate into Golgi cells and GABAergic DCN neurons in wild-type mice. The cells expressing p57 in the developing cerebellum at E12.5 are therefore likely precursors of Pax2-positive cells or a cell population that is closely related to Pax2-positive cells. Furthermore, massive

FIG. 2. Severe hydrocephalus as a result of p57 ablation specifically in the central nervous system. (A) PCR analysis of genomic DNA from the brains of mice of the indicated genotypes at P15. The positions of amplified fragments corresponding to wild-type (WT), floxed, and deleted (Δ) alleles are indicated. (B) RT and real-time PCR analysis of p57 mRNA in the brains of mice of the indicated genotypes at E13.5. Normalized data are expressed relative to the corresponding value for control mice and are means ± SD ($n = 3$ mice of each genotype). (C) Immunoblot (IB) analysis of p57 in the brains of mice of the indicated genotypes at E13.5. (D) Hematoxylin-eosin staining of the lenses of mice of the indicated genotypes at E16.5. Scale bars, 100 μm. (E) Gross appearance of nestin-Cre/*Kip2*$^{[+]/+}$ and nestin-Cre/*Kip2*$^{[+]/F}$ mice at P15. The arrow indicates the outspread cranium. Scale bar, 5 mm. (F) Body weights of control ($n = 31$) and nestin-Cre/*Kip2*$^{[+]/F}$ ($n = 12$) mice at P15. *, $P = 3.56 \times 10^{-11}$. (G) Kaplan-Meier plot of the overall rates of survival of control ($n = 38$) and nestin-Cre/*Kip2*$^{[+]/F}$ ($n = 13$) mice. (H) Hematoxylin-eosin staining of coronal sections of the forebrains from nestin-Cre/*Kip2*$^{[+]/+}$ and nestin-Cre/*Kip2*$^{[+]/F}$ mice at P15. Scale bar, 1 mm. (I) Hematoxylin-eosin staining of coronal sections of the SCOs in nestin-Cre/*Kip2*$^{[+]/+}$ and nestin-Cre/*Kip2*$^{[+]/F}$ mice at P5. The arrow indicates the abnormal SCO, and arrowheads indicate ependymal denudation in the lateral region for the mutant. Scale bar, 50 μm. (J) Immunofluorescence staining of p57 in the SCOs of nestin-Cre/*Kip2*$^{[+]/+}$ and nestin-Cre/*Kip2*$^{[+]/F}$ mice at E14.5. Cell nuclei were stained with Hoechst 33258. Scale bar, 25 μm. (K) Hematoxylin-eosin staining of coronal sections of the cerebral cortices in nestin-Cre/*Kip2*$^{[+]/+}$ and nestin-Cre/*Kip2*$^{[+]/F}$ mice at E18.5. Scale bar, 50 μm.

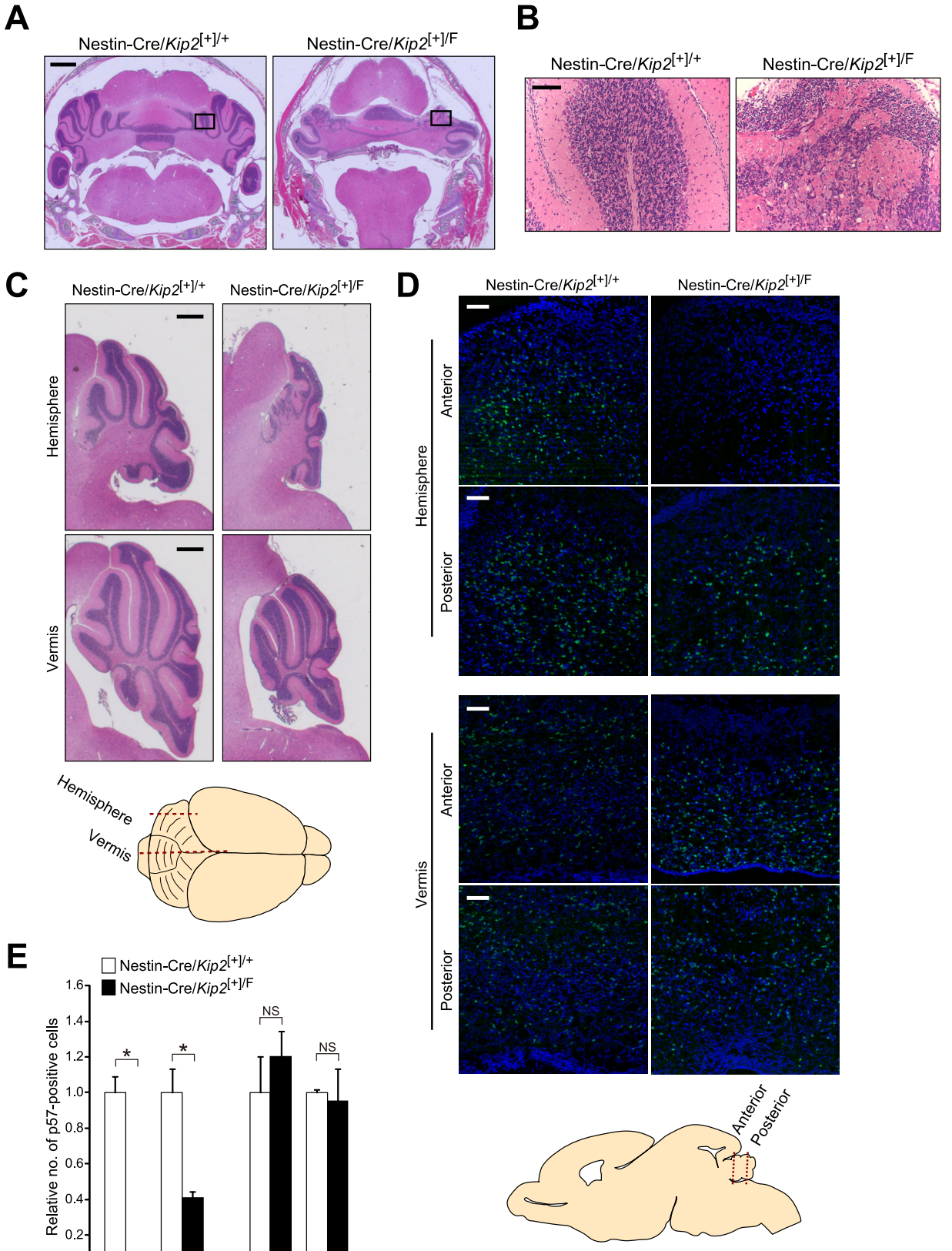
A
Nestin-Cre/Kip2[+]/+
Nestin-Cre/Kip2[+]/F
B
Nestin-Cre/Kip2[+]/+
Nestin-Cre/Kip2[+]/F
C
Nestin-Cre/Kip2[+]/+
Nestin-Cre/Kip2[+]/F
Hemisphere
Vermis
Hemisphere
Vermis
D
Nestin-Cre/Kip2[+]/+
Nestin-Cre/Kip2[+]/F
Hemisphere
Anterior
Posterior
Vermis
Anterior
Posterior
Anterior
Posterior
E
Nestin-Cre/Kip2[+]/+
Nestin-Cre/Kip2[+]/F
Relative no. of p57-positive cells
1.6
1.4
1.2
1.0
0.8
0.6
0.4
0.2
0
*
*
NS
NS
Anterior
Posterior
Anterior
Posterior
Hemisphere
Vermis

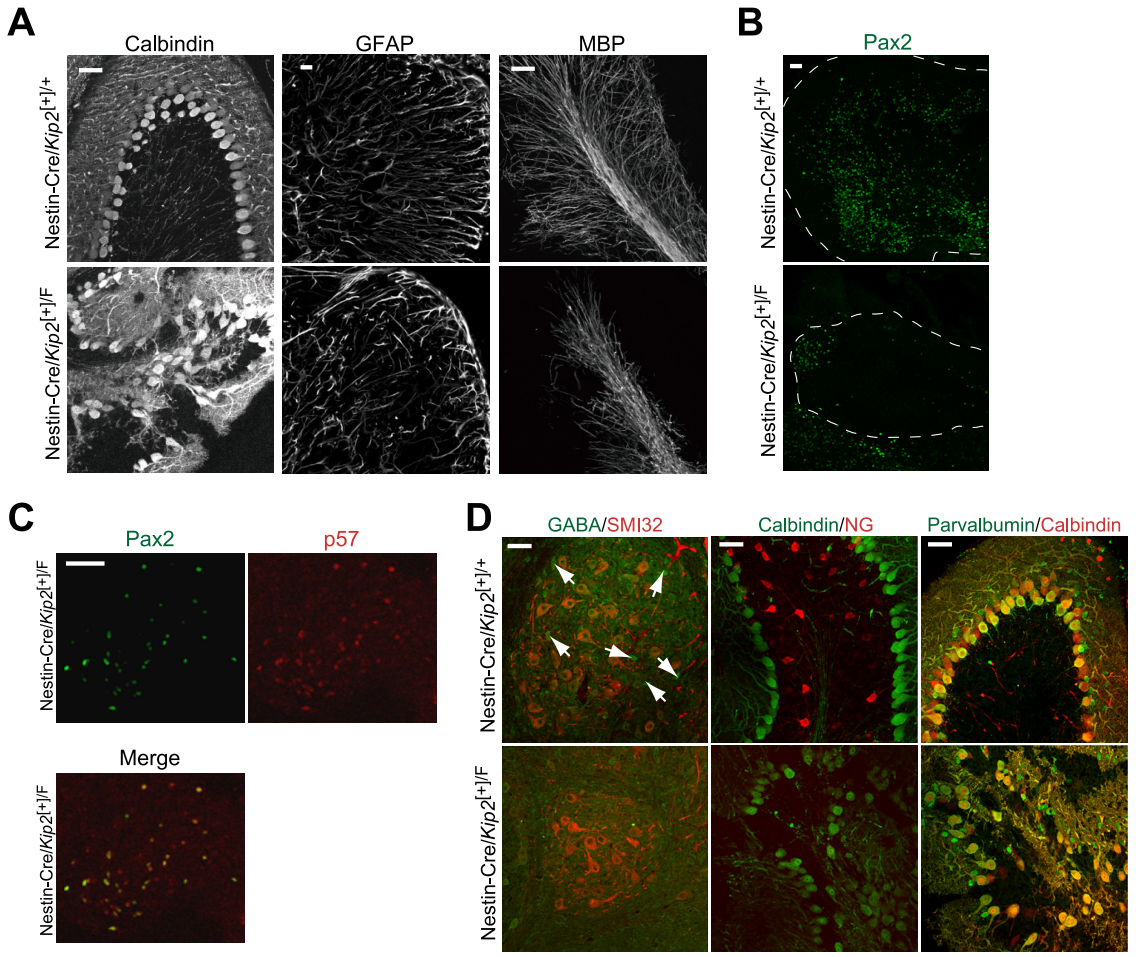

FIG. 4. Loss of Pax2-positive cells in the cerebella of p57-deficient mice. (A) Immunohistofluorescence analysis of calbindin, GFAP, and MBP in the cerebella of nestin-Cre/*Kip2*$^{[+]/+}$ and nestin-Cre/*Kip2*$^{[+]/F}$ mice at P15. Sagittal sections from the anterior lobe of the hemisphere are shown. Scale bars, 50 μm. (B to D) The cerebella of nestin-Cre/*Kip2*$^{[+]/+}$ and nestin-Cre/*Kip2*$^{[+]/F}$ mice were subjected to immunofluorescence staining with antibodies to Pax2 at P0 (B), with antibodies to Pax2 and to p57 at P0 (C), or with antibodies to the indicated proteins at P15 (D). Arrows indicate GABAergic DCN neurons. Coronal sections from the anterior lobe of the hemisphere are shown in panels B and C. (D) Sagittal sections from deep cerebellar nuclei are shown for GABA/SMI32 staining, and those from the anterior lobe of the hemisphere are shown for calbindin/neurogranin (NG) and parvalbumin/calbindin staining. Scale bars, 50 μm.

apoptosis during midembryogenesis is likely responsible for the loss of Golgi cells and GABAergic DCN neurons in nestin-Cre/*Kip2*$^{[+]/F}$ mice.

Additional deletion of *Tp53* prevents hydrocephalus and cerebellar malformation. Given that the amounts of mRNAs for p21 and Noxa, both of which are downstream targets of p53, were increased in the brains of nestin-Cre/*Kip2*$^{[+]/F}$ mice (Fig. 7A), we investigated the possible role of p53 in the abnormal induction of apoptosis in these animals. We thus crossed nestin-Cre/*Kip2*$^{[+]/F}$ mice with *Tp53*$^{-/-}$ mice to generate animals that lack both p57 and p53 in the brain. Nestin-Cre/*Kip2*$^{[+]/F}$/*Tp53*$^{-/-}$ mice were viable and indistinguishable from wild-type mice, at least within the first 3 months after birth, and they thus did not manifest hydrocephalus or cerebellar malformation (Fig. 7B and C). Furthermore, nestin-Cre/*Kip2*$^{[+]/F}$/*Tp53*$^{+/-}$ mice also exhibited substantial re-

FIG. 3. Cerebellar malformation in the cerebella of p57-deficient mice. (A and B) Hematoxylin-eosin staining of coronal sections of the cerebella from nestin-Cre/*Kip2*$^{[+]/+}$ and nestin-Cre/*Kip2*$^{[+]/F}$ mice at P15. The boxed regions in panel A are shown at higher magnification in panel B. Scale bars, 1 mm (A) and 100 μm (B). (C) Hematoxylin-eosin staining of sagittal sections of the indicated regions of the cerebella from nestin-Cre/*Kip2*$^{[+]/+}$ and nestin-Cre/*Kip2*$^{[+]/F}$ mice at P15. A schematic representation of the brain is also shown, with the dashed red lines indicating the positions of the sections. Scale bars, 500 μm. (D) Immunofluorescence staining of p57 (green) in the indicated regions of the cerebella from nestin-Cre/*Kip2*$^{[+]/+}$ and nestin-Cre/*Kip2*$^{[+]/F}$ mice at P0.5. Nuclei were stained with Hoechst 33258 (blue). A schematic representation of the cerebellum is also shown, with the dashed red lines indicating the positions of the sections. Scale bars, 50 μm. (E) Quantitative analysis of cells positive for p57 in images similar to those in panel D. Data are expressed relative to the corresponding control value and are means ± SD ($n = 3$). *, $P < 0.005$; NS, not significant.

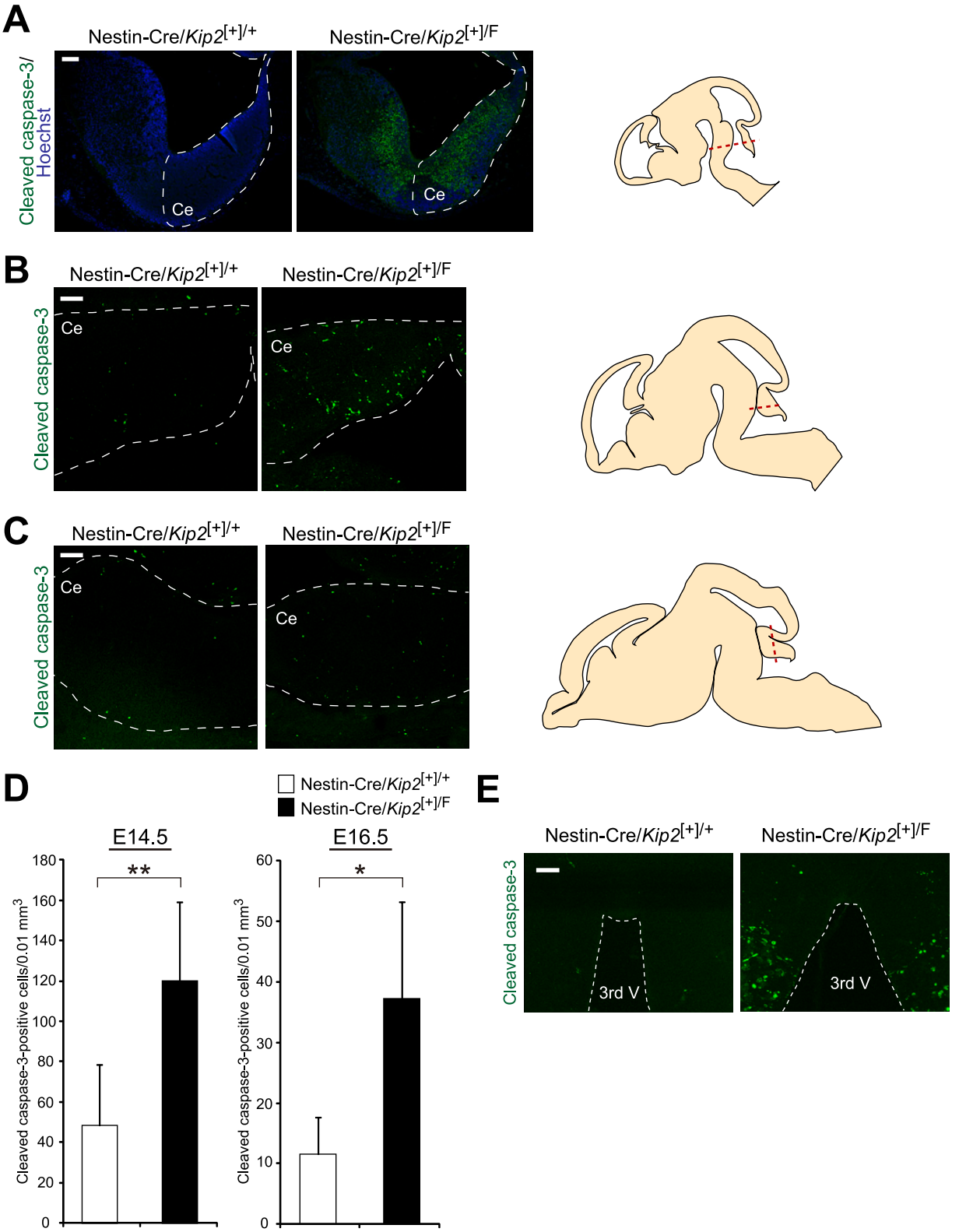

FIG. 5. Massive apoptosis in the cerebellar primordium induced by p57 ablation. (A to C) Immunofluorescence staining of cleaved caspase-3 in the cerebella of nestin-Cre/*Kip2*$^{[+]/+}$ and nestin-Cre/*Kip2*$^{[+]/F}$ mice at E12.5 (A), E14.5 (B), and E16.5 (C). Horizontal sections (A and B) and coronal sections (C) of the cerebellar primordium are shown. Dashed lines demarcate the cerebellar primordium (Ce). Cell nuclei in panel A were stained with Hoechst 33258. Schematic representations of the brain are also shown, with dashed red lines indicating the positions of the sections. Scale bars, 100 μm. (D) Quantitative analysis of cells positive for cleaved caspase-3 in images similar to those in panels B and C. Data are means ± SD (n = 4 independent experiments). *, P = 0.003; **, P = 0.0006. (E) Immunofluorescence staining of cleaved caspase-3 in coronal sections of the SCOs of nestin-Cre/*Kip2*$^{[+]/+}$ and nestin-Cre/*Kip2*$^{[+]/F}$ mice at E14.5. 3rd V, third ventricle. Scale bar, 50 μm.

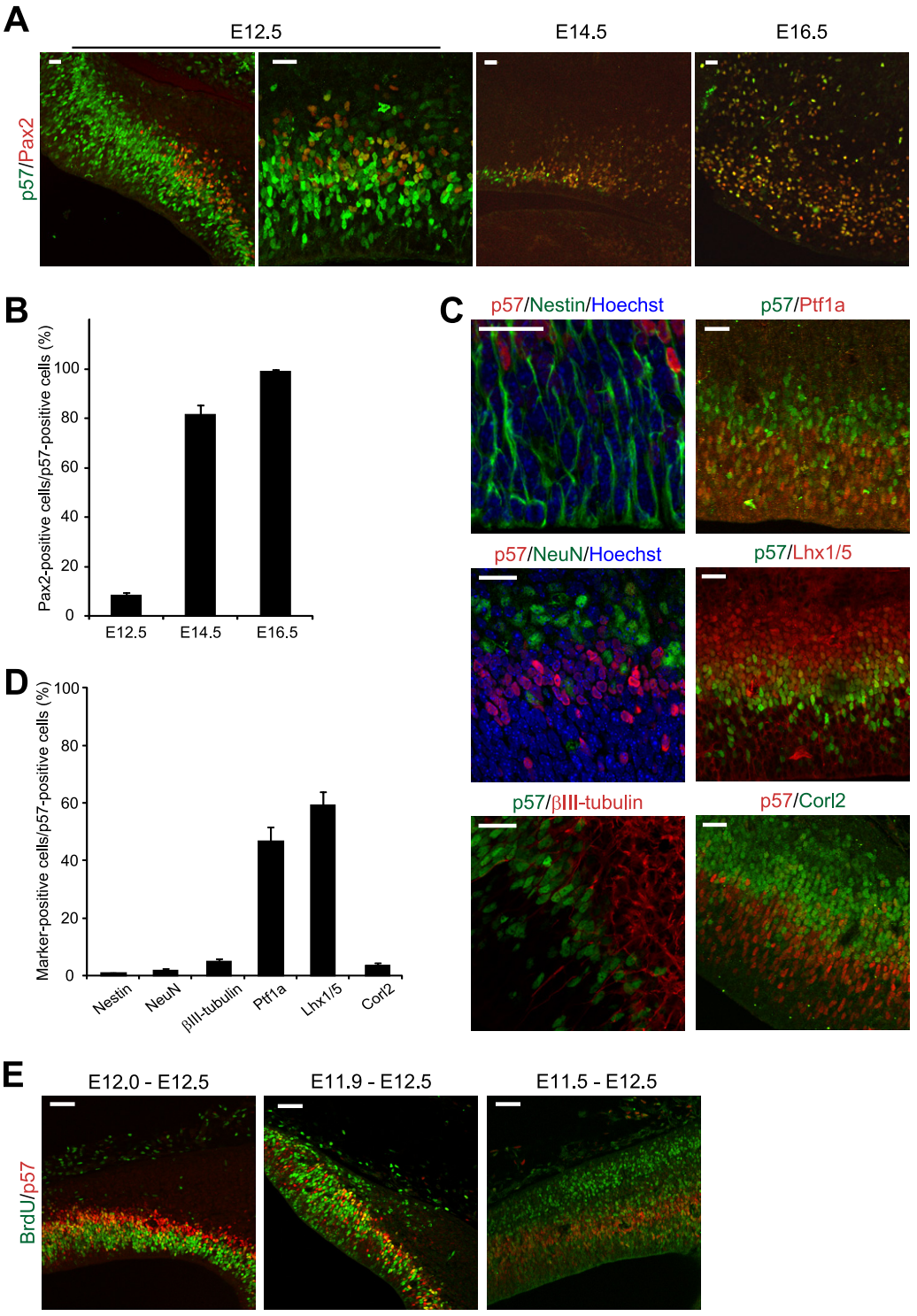

FIG. 6. Characterization of p57-positive cells in the cerebellar primordium. (A) Immunofluorescence staining of p57 and Pax2 in the cerebella of wild-type mice at E12.5, E14.5, and E16.5. Scale bars, 25 μm. (B) Quantitative analysis of cells positive for Pax2 among p57-positive cells in images similar to those in panel A. Data are means ± SD ($n = 3$). (C) Characterization of p57-expressing cells in the cerebella of wild-type mice at E12.5 by immunofluorescence staining with antibodies to p57 and to the indicated proteins. Scale bars, 25 μm. (D) Quantitative analysis of cells positive for each marker among p57-positive cells in images similar to those in panel C. Data are means ± SD ($n = 3$). (E) Immunofluorescence staining of BrdU and p57 in the cerebella of wild-type mice at E12.5 after BrdU administration at the indicated times. Scale bars, 50 μm.

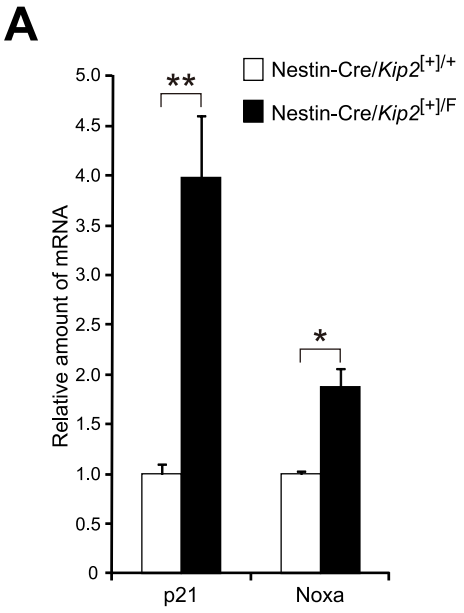

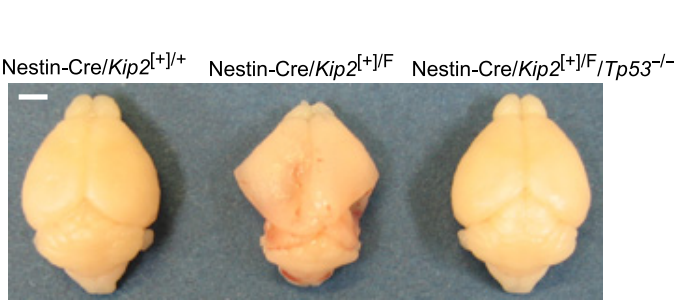

C

		Recovery ratio at P15	
		Hydrocephalus	Cerebellar malformation
Nestin-Cre/*Kip2*[+]/F	*Tp53*+/+	0/8 (0%)	0/8 (0%)
	Tp53+/−	12/14 (85.7%)	12/14 (85.7%)
	Tp53−/−	5/5 (100%)	5/5 (100%)

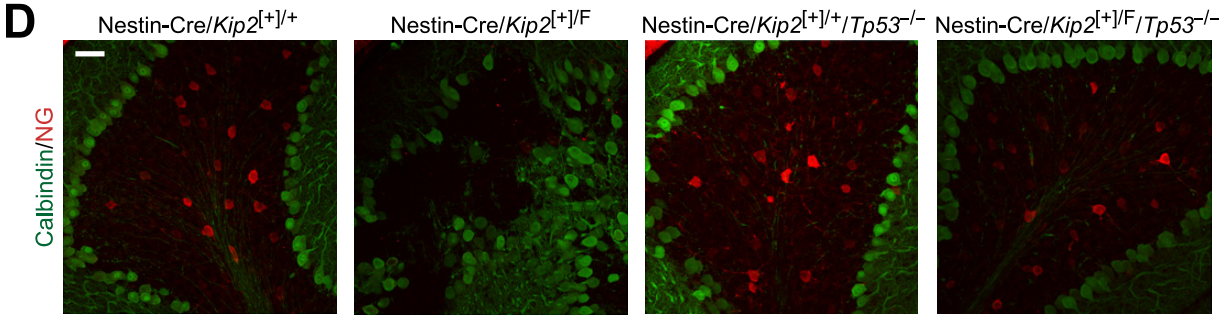

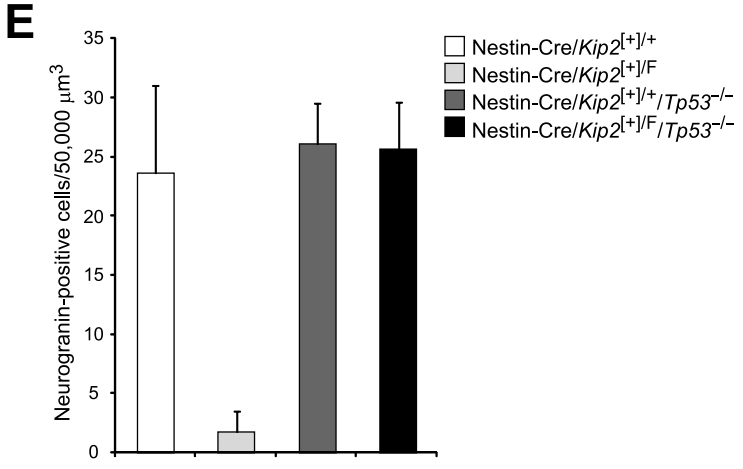

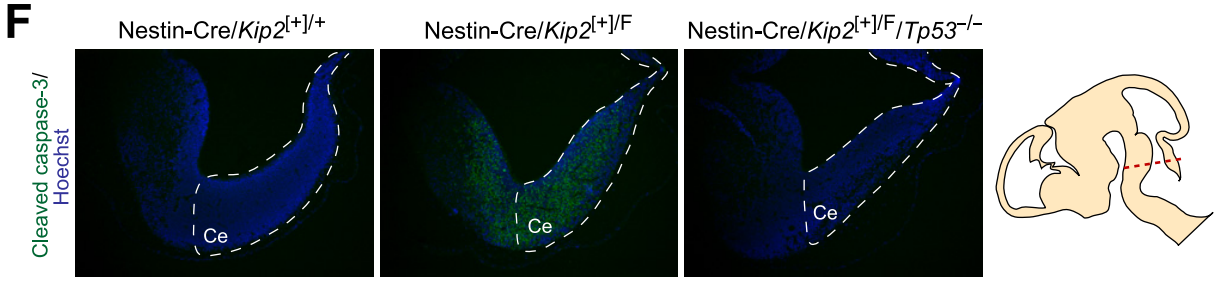

covery with regard to these anatomic abnormalities. Immunofluorescence analysis revealed that the layered organization of the cerebella and number of Golgi cells appeared normal in nestin-Cre/*Kip2*$^{[+]/F}$/*Tp53*$^{-/-}$ mice at P15 (Fig. 7D and E). We also found that the increased level of apoptosis apparent in nestin-Cre/*Kip2*$^{[+]/F}$ mice at E12.5 was normalized in nestin-Cre/*Kip2*$^{[+]/F}$/*Tp53*$^{-/-}$ mice (Fig. 7F). The cellular compositions of adult cerebella also did not differ substantially between nestin-Cre/*Kip2*$^{[+]/F}$/*Tp53*$^{-/-}$ and control mice (data not shown), suggesting that all developmental defects in nestin-Cre/*Kip2*$^{[+]/F}$ mice are attributable to the increased level of apoptosis rather than to other mechanisms, such as skewed cellular differentiation or a defect in cell migration. Collectively, our results suggested that the loss of p57 results in aberrant apoptosis in the SCO and cerebellum during development in a manner dependent on p53.

p57 function in brain development is replaceable by p27. Whereas the members of the Cip/Kip family of CKIs (p21, p27, and p57) share a CKI domain that is essential for inhibition of CDKs, p57 also contains a central domain that is absent in p21 and p27 and is thought to mediate functions other than inhibition of CDKs (17). To test whether p57 function in brain development is replaceable by p27, we examined the brains of *Kip2*$^{[+]/Kip1KI}$ mice, in which the expressed allele of the p57 gene has been replaced with the p27 gene (31, 32). We first examined the expression of p27 in the cerebella of *Kip2*$^{[+]/+}$ and *Kip2*$^{[+]/Kip1KI}$ mice at P0.5 (Fig. 8A). Whereas few Pax2-positive cells in the cerebella of *Kip2*$^{[+]/+}$ mice expressed p27, p27 appeared to be expressed in most Pax2-positive cells in the cerebella of *Kip2*$^{[+]/Kip1KI}$ mice. The gross appearance of the brains of *Kip2*$^{[+]/Kip1KI}$ mice was indistinguishable from that of wild-type mice (Fig. 8B), and there was no sign of increased intracranial pressure associated with hydrocephalus (Fig. 8C and D). Microscopic examination of cerebellar structure did not reveal any morphological abnormalities in *Kip2*$^{[+]/Kip1KI}$ mice (Fig. 8C and E). Furthermore, the number of Golgi cells, which are mostly absent in nestin-Cre/*Kip2*$^{[+]/F}$ mice, appeared unchanged in *Kip2*$^{[+]/Kip1KI}$ mice from the number in control animals (Fig. 8F). We also generated nestin-Cre/*Kip2*$^{[+]/F}$/*Kip1*$^{-/-}$ mice, in which both p57 and p27 are absent in the brain. The double mutant mice died immediately after birth, whereas most nestin-Cre/*Kip2*$^{[+]/F}$ mice survived for 2 to 3 weeks after birth (Fig. 8G). Histopathologic examination did not reveal any large defects that might account for this neonatal mortality (data not shown), the reason for which awaits further clarification.

We further examined whether the loss of Pax2-positive cells was also apparent in the cerebella of constitutive p57 knockout (*Kip2*$^{[+]/-}$) mice. Whereas p57 ablation resulted in the loss of Pax2-positive cells in the conditional knockout mice, such a loss was not obvious in the cerebella of the constitutive knockout mice (Fig. 9A). The abundance of p27 mRNA was increased in the brains of constitutive p57 knockout mice at E12.5, whereas such upregulation of p27 mRNA was not observed in nestin-Cre/*Kip2*$^{[+]/F}$ mice (Fig. 9B and C). These results therefore suggested that p27 might compensate in part for the chronic p57 deficiency in constitutive p57 knockout mice but not for the acute inactivation of p57 in nestin-Cre/*Kip2*$^{[+]/F}$ mice. Collectively, these results suggested that the total amount of CKIs is an important determinant of brain development, although p57 appears to be especially important in regions of the brain such as those containing DCN neurons and Golgi cells. The phenotype of the p57-deficient brain is thus likely attributable to an increase in CDK activity that results from the loss of the CKI function of p57.

The increased activity of E2F1 contributes to the phenotype of the p57-deficient brain. Finally, we investigated how increased CDK activity might trigger p53-dependent apoptosis, focusing on the possible contribution of the retinoblastoma protein (Rb)-E2F pathway. The excessive activity of E2F1 was previously shown to induce p53-dependent or -independent apoptosis in a manner dependent on cellular context (4, 14, 26, 27). Phosphorylation of Rb in the brains of nestin-Cre/*Kip2*$^{[+]/F}$ mice at E12.5 was increased compared with that in control mice (Fig. 10A). We also examined the expression of E2F target genes in p57-deficient brains at E12.5 (Fig. 10B). Expression of the genes for Mcm3, Cdc6, and Cdt1, all of which are E2F targets related to the cell cycle, was moderately but significantly increased. In addition, expression of the gene for p73, which is an E2F target related to apoptosis, was markedly increased. These results thus indicated that E2F activity is indeed increased by ablation of p57 in the brain. We next crossed nestin-Cre/*Kip2*$^{[+]/F}$ mice with *E2f1*$^{-/-}$ mice to generate animals that lack both p57 and E2F1 in their brains. Nestin-Cre/*Kip2*$^{[+]/F}$/*E2f1*$^{-/-}$ mice manifested recovery from the defects of nestin-Cre/*Kip2*$^{[+]/F}$ mice, including hydrocephalus, cerebellar malformation, and loss of Golgi cells, although the penetrance of such recovery did not reach 40% (Fig. 10C to E), suggesting that other members of the E2F family might contribute to the abnormalities of nestin-Cre/*Kip2*$^{[+]/F}$ mice. We therefore concluded that the loss of p57 in the brain results in excessive E2F activity, which in turn induces p53-dependent

FIG. 7. Reversal of the abnormalities of the p57-deficient brain by additional ablation of p53. (A) RT and real-time PCR analysis of mRNAs derived from p53 target genes in the brains of nestin-Cre/*Kip2*$^{[+]/+}$ and nestin-Cre/*Kip2*$^{[+]/F}$ mice at E12.5. Normalized data are expressed relative to the corresponding value for control mice and are means ± SD ($n = 4$ mice of each genotype). *, $P < 0.001$; **, $P < 0.0001$. (B) Gross appearance of the brains of nestin-Cre/*Kip2*$^{[+]/+}$, nestin-Cre/*Kip2*$^{[+]/F}$, and nestin-Cre/*Kip2*$^{[+]/F}$/*Tp53*$^{-/-}$ mice at P15. Scale bar, 2.5 mm. (C) Summary of the recovery rate for hydrocephalus and cerebellar malformation in mice of the indicated genotypes at P15. (D) Immunofluorescence staining of the cerebella of nestin-Cre/*Kip2*$^{[+]/+}$, nestin-Cre/*Kip2*$^{[+]/F}$, nestin-Cre/*Kip2*$^{[+]/+}$/*Tp53*$^{-/-}$, and nestin-Cre/*Kip2*$^{[+]/F}$/*Tp53*$^{-/-}$ mice at P15 with antibodies to calbindin and to neurogranin (NG). Sagittal sections from the anterior lobe of the hemisphere are shown. Scale bar, 50 μm. (E) Quantitative analysis of Golgi cells. The cerebella of nestin-Cre/*Kip2*$^{[+]/+}$, nestin-Cre/*Kip2*$^{[+]/F}$, nestin-Cre/*Kip2*$^{[+]/+}$/*Tp53*$^{-/-}$, and nestin-Cre/*Kip2*$^{[+]/F}$/*Tp53*$^{-/-}$ mice at P15 were subjected to immunofluorescence staining with antibodies to neurogranin, and the number of neurogranin-positive cells in the granule cell layer was counted. Data are means ± SD ($n = 4$ independent experiments). (F) Immunofluorescence staining of cleaved caspase-3 in horizontal sections of the cerebella from nestin-Cre/*Kip2*$^{[+]/+}$, nestin-Cre/*Kip2*$^{[+]/F}$, and nestin-Cre/*Kip2*$^{[+]/F}$/*Tp53*$^{-/-}$ mice at E12.5. Cell nuclei were stained with Hoechst 33258. Dashed lines demarcate the cerebellar primordium (Ce). A schematic representation of the brain is also shown, with the dashed red line indicating the position of the sections. Scale bar, 100 μm.

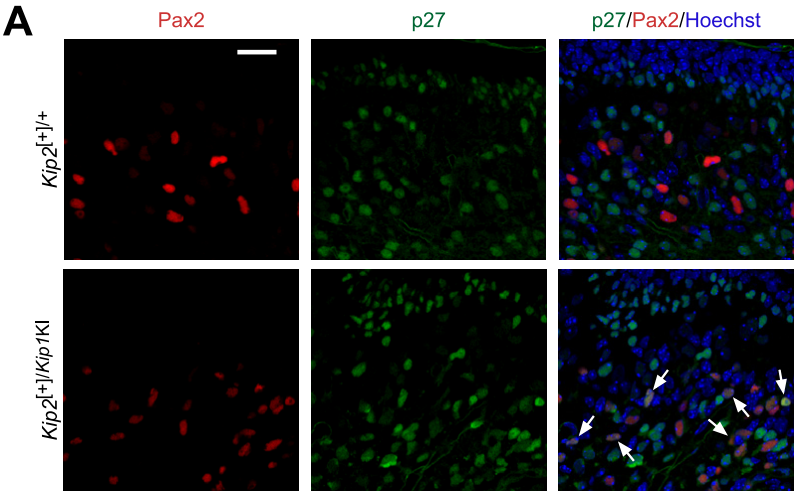

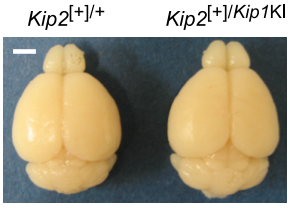

C

Recovery ratio in $Kip2^{[+]/Kip1KI}$ mice at P15	
Hydrocephalus	9/9 (100%)
Cerebellar malformation	9/9 (100%)

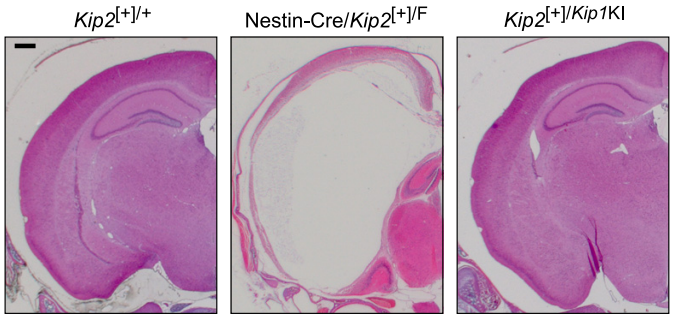

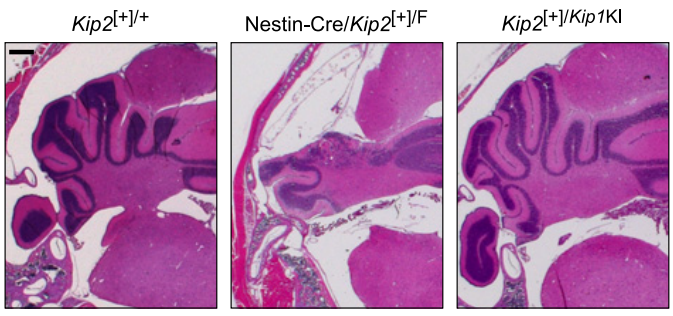

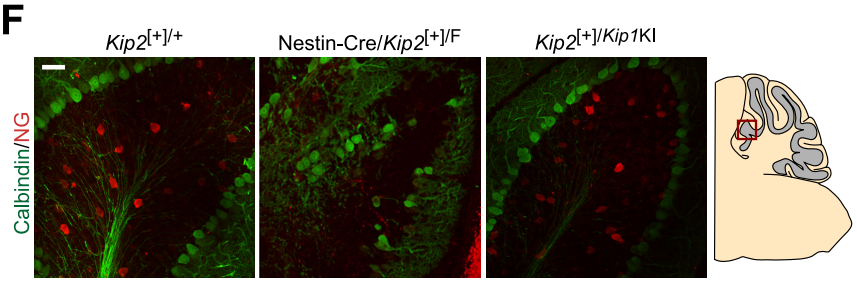

G

		Ratio of death at birth	
Nestin-Cre/$Kip2^{[+]/F}$	$Kip1^{+/+}$	2/7	(28.6%)
	$Kip1^{+/-}$	2/14	(14.3%)
	$Kip1^{-/-}$	6/6	(100%)

FIG. 8. Normalization of the phenotype of the p57-deficient brain by p27 knock-in. (A) Immunofluorescence staining of p27 and Pax2 in the cerebella of $Kip2^{[+]/+}$ (wild-type) and $Kip2^{[+]/Kip1KI}$ mice at P0.5. Arrows indicate cells with a high level of p27 expression. Scale bar, 100 μm. (B) Gross appearance of the brains of $Kip2^{[+]/+}$ and $Kip2^{[+]/Kip1KI}$ mice at P25. Scale bar, 2 mm. (C) Summary of the recovery rate for hydrocephalus and cerebellar malformation in $Kip2^{[+]/Kip1KI}$ mice at P15. (D and E) Hematoxylin-eosin staining of coronal sections of the forebrains (D) and cerebella (E) of $Kip2^{[+]/+}$, nestin-Cre/$Kip2^{[+]/F}$, and $Kip2^{[+]/Kip1KI}$ mice at P15. Scale bars, 500 μm. (F) Immunofluorescence staining of the cerebella of $Kip2^{[+]/+}$, nestin-Cre/$Kip2^{[+]/F}$, and $Kip2^{[+]/Kip1KI}$ mice at P15 with antibodies to calbindin and to neurogranin (NG). A schematic representation of the cerebellum is also shown, with the red box indicating the position of the sections. Scale bar, 50 μm. (G) Summary of the ratios of death immediately after birth for mice of the indicated genotypes.

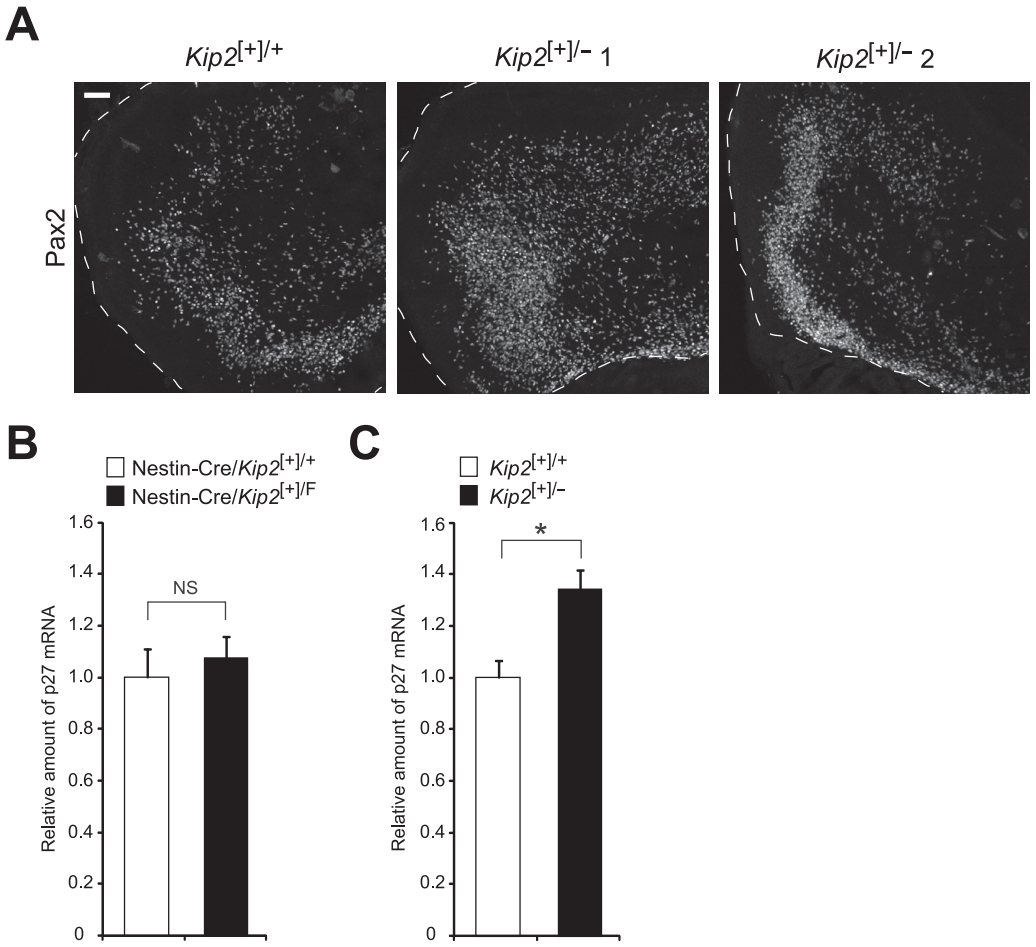

FIG. 9. Brain phenotype of conventional p57 knockout mice. (A) Immunostaining of Pax2 in the cerebella (demarcated by the dashed line) of $Kip2^{[+]/+}$ and $Kip2^{[+]/-}$ mice at E18.5. Sections from two different $Kip2^{[+]/-}$ mice are shown. Scale bar, 100 μm. (B and C) RT and real-time PCR analysis of p27 mRNA in the brains of nestin-Cre/$Kip2^{[+]/+}$ and nestin-Cre/$Kip2^{[+]/F}$ (B) and of $Kip2^{[+]/+}$ and $Kip2^{[+]/-}$ (C) mice at E12.5. Normalized data are expressed relative to the corresponding values for control mice and are means ± SD ($n = 4$ mice of each genotype). *, $P < 0.01$.

apoptosis, finally leading to hydrocephalus and cerebellar malformation.

DISCUSSION

We have elucidated the physiological importance of p57 during brain development by analysis of the effects of brain-specific deletion of the p57 gene in mice. The mutant mice manifested severe nonobstructive hydrocephalus and cerebellar malformation, which appear to be attributable to an increased level of apoptosis during midembryogenesis. This apoptosis is dependent on the E2F-p53 axis, given that additional ablation of either E2F1 or p53 in brain-specific p57-deficient mice prevented both hydrocephalus and the cerebellar anomaly. We thus propose that the loss of p57 results in hyperactivation of E2F and the consequent induction of p53-dependent apoptosis.

The related CKIs p27 and p57 differ in the times and places of their expression in many tissues and organs, including the brain (22). In the cerebellum, p27 is expressed mostly in granule cells (glutamatergic excitatory neurons) after birth (21). In contrast, p57 is expressed predominantly in Pax2-positive cells, which are precursors of GABAergic inhibitory neurons, from midembryogenesis to the neonatal period. The effects of p27 or p57 gene deletion in the cerebellum thus also differ: p27 deficiency results in hyperproliferation of granule cells during adulthood (21), whereas p57 deficiency results in the apoptosis of Pax2-positive interneuron precursors during embryogenesis. Nevertheless, the defects induced by p57 deficiency were reversed by p27 knock-in, suggesting that the molecular roles of these CKIs are indistinguishable. The specific response of cells to the lack of each CKI is therefore dependent on cell type rather than on CKI type. This relation between p27 and p57 in the brain is similar to that observed in most (but not all) other tissues (31, 32).

In regions of the central nervous system other than the cerebellum, p57 is expressed predominantly in the SCO, the subventricular and mantle zones of the hippocampus, the septum, the basal ganglia, the thalamus, the hypothalamus, the midbrain, and the spinal cord from E12.5 to E16.5 (2, 6, 39). The expression of p57 precedes that of p27 as cells undergo differentiation, and a subset of cells expresses both p27 and

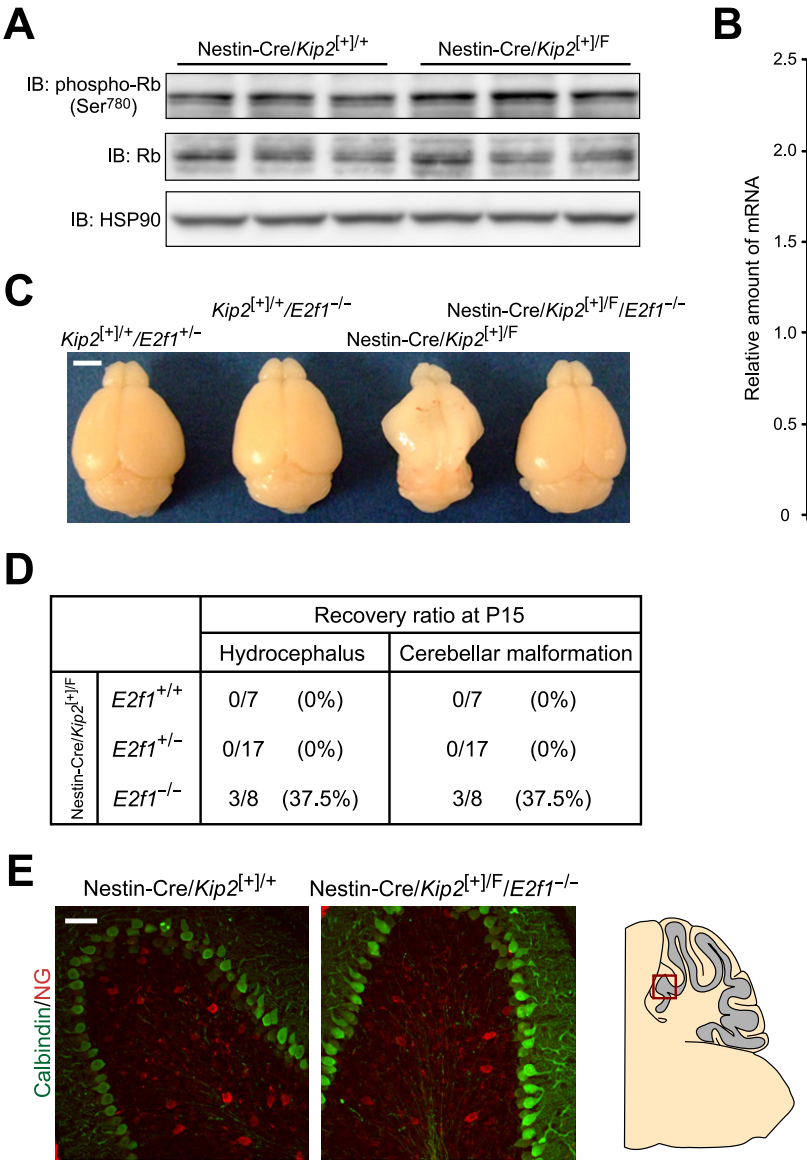

FIG. 10. Role of E2F1 in the action of the p57-p53 axis in brain development. (A) Immunoblot (IB) analysis of Rb and phosphorylated Rb in the brains of nestin-Cre/*Kip2*$^{[+]/+}$ and nestin-Cre/*Kip2*$^{[+]/F}$ mice at E12.5. Each lane corresponds to a different animal. (B) RT and real-time PCR analysis of mRNAs derived from E2F target genes in the brains of nestin-Cre/*Kip2*$^{[+]/+}$ and nestin-Cre/*Kip2*$^{[+]/F}$ mice at E12.5. Normalized data are expressed relative to the corresponding values for control mice and are means ± SD ($n = 3$ mice of each genotype). *, $P < 0.05$; **, $P < 0.005$. (C) Gross appearance of the brains of mice of the indicated genotypes at P15. Scale bar, 2.5 mm. (D) Summary of the recovery rates from hydrocephalus and cerebellar malformation for mice of the indicated genotypes at P15. (E) Immunofluorescence staining of the cerebella of nestin-Cre/*Kip2*$^{[+]/+}$ and nestin-Cre/*Kip2*$^{[+]/F}$/*E2f1*$^{-/-}$ mice at P15 with antibodies to calbindin and to neurogranin (NG). A schematic representation of the cerebellum is also shown, with the red box indicating the position of the sections. Scale bar, 50 μm.

p57, suggesting potentially related yet distinct functions of Cip/Kip family members during neurogenesis (2, 6, 39). This finding is consistent with our observation that mice lacking both p27 and p57 in the brain die immediately after birth. After E18.5, expression of p57 is limited to regions undergoing differentiation and ceases within a short period after birth.

One of the most prominent defects induced by ablation of p57 is the loss of Pax2-positive cells in the cerebellum. However, the detailed mechanism by which the loss of such cells results in cerebellar disorganization remains unclear. Appropriate interactions among multiple cell lineages are thought to be essential for formation of normal cerebellar architecture as well as for efficient cell proliferation. For example, Sonic hedgehog secreted from Purkinje cells promotes the proliferation of granule cells, which constitute a large subset of cerebellar neurons (35). The hypoplasia associated with the marked malformation of the cerebella in p57-deficient mice might therefore be attributable directly to the massive apoptosis observed during embryogenesis or to a proliferation defect resulting from the loss of such intercellular interactions (or both).

Most p57-positive cells in the cerebella of wild-type mice did not express Pax2 at E12.5, at which time maximal apoptosis was apparent in the p57-deficient mice. Although these p57-positive cells may be precursors of Pax2-positive cells, we are not able to exclude the possibility that they belong to a lineage other than Pax2-positive neuronal precursors but are essential for the development of the latter cells. Given that a large subset of p57-positive cells expresses Pax2 at E14.5, at which time the extent of apoptosis was still increased in the p57-deficient cerebellar primordium, most of the apoptotic cells in the mutant brain are likely Pax2-positive neuronal precursors. Further analysis is required to determine the lineage of the cells that undergo apoptosis in response to the loss of p57 in the brain.

The CKI p57 performs various biological functions in addition to inhibition of the cell cycle. First, p57 controls neural differentiation through transcriptional regulation. It directly interacts with the transcription factor Nurr1 and modulates its *trans*-activation activity, resulting in promotion of the differentiation of MN9D cells into dopaminergic neurons (12). It also binds to the product of the proneural gene *Mash1* and inhibits its potential for *trans* activation of target genes (11). These actions of p57 in transcriptional control are not dependent on CKI activity. Second, p57 (and also p27) functions in the regulation of neuronal migration in the cerebral cortex (9, 13, 25). These non-CKI functions of p57 might also contribute to cerebellar development. However, this seems unlikely because the brain abnormalities of p57-deficient mice were prevented by p27 knock-in or by additional ablation of p53 or E2F1. Our results thus support the notion that the cerebellar malformation associated with p57 deficiency is the result of a loss of the CKI activity of p57 rather than that of other non-CKI functions. Collectively, our data indicate that the p57-E2F-p53 axis is required for the normal development of a subset of neurons in the cerebellum.

ACKNOWLEDGMENTS

We thank L. Yamasaki for *E2f1*$^{-/-}$ mice, Y. Ono for antibodies to Corl2, D. R. Littman for pL2-Neo and pMC-Cre, A. Niihara, C. Mitai, Y. Yamada, K. Takeda, and M. Tanaka for technical assistance, members of our laboratories for comments on the manuscript, and A. Ohta and M. Kimura for help in preparation of the manuscript. The monoclonal antibodies to Lhx1/5 and nestin were obtained from the Developmental Studies Hybridoma Bank and were developed under the auspices of the National Institute of Child Health and Human Development and maintained at the Department of Biological Sciences, University of Iowa.

This work was supported in part by a grant from the Ministry of Education, Culture, Sports, Science and Technology of Japan.

REFERENCES

1. **Altman, J., and S. A. Bayer.** 1978. Prenatal development of the cerebellar system in the rat. I. Cytogenesis and histogenesis of the deep nuclei and the cortex of the cerebellum. J. Comp. Neurol. **179:**23–48.
2. **Bilodeau, S., A. Roussel-Gervais, and J. Drouin.** 2009. Distinct developmental roles of cell cycle inhibitors p57^{Kip2} and p27^{Kip1} distinguish pituitary progenitor cell cycle exit from cell cycle reentry of differentiated cells. Mol. Cell. Biol. **29:**1895–1908.
3. **Chizhikov, V. V., et al.** 2006. The roof plate regulates cerebellar cell-type specification and proliferation. Development **133:**2793–2804.
4. **DeGregori, J., G. Leone, A. Miron, L. Jakoi, and J. R. Nevins.** 1997. Distinct roles for E2F proteins in cell growth control and apoptosis. Proc. Natl. Acad. Sci. U. S. A. **94:**7245–7250.
5. **Forni, P. E., et al.** 2006. High levels of Cre expression in neuronal progenitors cause defects in brain development leading to microencephaly and hydrocephaly. J. Neurosci. **26:**9593–9602.
6. **Gui, H., S. Li, and M. P. Matise.** 2007. A cell-autonomous requirement for Cip/Kip cyclin-kinase inhibitors in regulating neuronal cell cycle exit but not differentiation in the developing spinal cord. Dev. Biol. **301:**14–26.
7. **Hevner, R. F., R. D. Hodge, R. A. Daza, and C. Englund.** 2006. Transcription factors in glutamatergic neurogenesis: conserved programs in neocortex, cerebellum, and adult hippocampus. Neurosci. Res. **55:**223–233.
8. **Hoshino, M., et al.** 2005. Ptf1a, a bHLH transcriptional gene, defines GABAergic neuronal fates in cerebellum. Neuron **47:**201–213.
9. **Itoh, Y., N. Masuyama, K. Nakayama, K. I. Nakayama, and Y. Gotoh.** 2007. The cyclin-dependent kinase inhibitors p57 and p27 regulate neuronal migration in the developing mouse neocortex. J. Biol. Chem. **282:**390–396.
10. **Jiménez, A. J., et al.** 2001. A programmed ependymal denudation precedes congenital hydrocephalus in the hyh mutant mouse. J. Neuropathol. Exp. Neurol. **60:**1105–1119.
11. **Joseph, B., et al.** 2009. p57^{Kip2} is a repressor of Mash1 activity and neuronal differentiation in neural stem cells. Cell Death Differ. **16:**1256–1265.
12. **Joseph, B., et al.** 2003. p57^{Kip2} cooperates with Nurr1 in developing dopamine cells. Proc. Natl. Acad. Sci. U. S. A. **100:**15619–15624.
13. **Kawauchi, T., K. Chihama, Y. Nabeshima, and M. Hoshino.** 2006. Cdk5 phosphorylates and stabilizes p27^{kip1} contributing to actin organization and cortical neuronal migration. Nat. Cell Biol. **8:**17–26.
14. **Kowalik, T. F., J. DeGregori, J. K. Schwarz, and J. R. Nevins.** 1995. E2F1 overexpression in quiescent fibroblasts leads to induction of cellular DNA synthesis and apoptosis. J. Virol. **69:**2491–2500.
15. **Maricich, S. M., and K. Herrup.** 1999. Pax-2 expression defines a subset of GABAergic interneurons and their precursors in the developing murine cerebellum. J. Neurobiol. **41:**281–294.
16. **Matsumoto, A., et al.** p57 is required for quiescence and maintenance of adult hematopoietic stem cells. Cell Stem Cell, in press.
17. **Matsuoka, S., et al.** 1995. p57^{KIP2}, a structurally distinct member of the p21^{CIP1} Cdk inhibitor family, is a candidate tumor suppressor gene. Genes Dev. **9:**650–662.
18. **Meiniel, A.** 2007. The secretory ependymal cells of the subcommissural organ: which role in hydrocephalus? Int. J. Biochem. Cell Biol. **39:**463–468.
19. **Miale, I. L., and R. L. Sidman.** 1961. An autoradiographic analysis of histogenesis in the mouse cerebellum. Exp. Neurol. **4:**277–296.
20. **Minaki, Y., T. Nakatani, E. Mizuhara, T. Inoue, and Y. Ono.** 2008. Identification of a novel transcriptional corepressor, Corl2, as a cerebellar Purkinje cell-selective marker. Gene Expr. Patterns **8:**418–423.
21. **Miyazawa, K., et al.** 2000. A role for p27/Kip1 in the control of cerebellar granule cell precursor proliferation. J. Neurosci. **20:**5756–5763.
22. **Nagahama, H., et al.** 2001. Spatial and temporal expression patterns of the cyclin-dependent kinase (CDK) inhibitors p27^{Kip1} and p57^{Kip2} during mouse development. Anat. Embryol. **203:**77–87.
23. **Nakayama, K., et al.** 1996. Mice lacking p27^{Kip1} display increased body size, multiple organ hyperplasia, retinal dysplasia, and pituitary tumors. Cell **85:**707–720.
24. **Nakayama, K., et al.** 2000. Targeted disruption of *Skp2* results in accumulation of cyclin E and p27^{Kip1}, polyploidy and centrosome overduplication. EMBO J. **19:**2069–2081.
25. **Nguyen, L., et al.** 2006. p27^{kip1} independently promotes neuronal differentiation and migration in the cerebral cortex. Genes Dev. **20:**1511–1524.
26. **Phillips, A. C., S. Bates, K. M. Ryan, K. Helin, and K. H. Vousden.** 1997. Induction of DNA synthesis and apoptosis are separable functions of E2F-1. Genes Dev. **11:**1853–1863.
27. **Qin, X. Q., D. M. Livingston, W. G. Kaelin, Jr., and P. D. Adams.** 1994. Deregulated transcription factor E2F-1 expression leads to S-phase entry and p53-mediated apoptosis. Proc. Natl. Acad. Sci. U. S. A. **91:**10918–10922.
28. **Sakakibara, S., et al.** 2002. RNA-binding protein Musashi family: roles for CNS stem cells and a subpopulation of ependymal cells revealed by targeted disruption and antisense ablation. Proc. Natl. Acad. Sci. U. S. A. **99:**15194–15199.
29. **Sillitoe, R. V., and A. L. Joyner.** 2007. Morphology, molecular codes, and circuitry produce the three-dimensional complexity of the cerebellum. Annu. Rev. Cell Dev. Biol. **23:**549–577.
30. **Sotelo, C.** 2004. Cellular and genetic regulation of the development of the cerebellar system. Prog. Neurobiol. **72:**295–339.
31. **Susaki, E., K. Nakayama, L. Yamasaki, and K. I. Nakayama.** 2009. Common and specific roles of the related CDK inhibitors p27 and p57 revealed by a knock-in mouse model. Proc. Natl. Acad. Sci. U. S. A. **106:**5192–5197.
32. **Susaki, E., and K. I. Nakayama.** 2009. Functional similarities and uniqueness of p27 and p57: insight from a knock-in mouse model. Cell Cycle **8:**2497–2501.
33. **Takahashi, K., K. Nakayama, and K. I. Nakayama.** 2000. Mice lacking a CDK inhibitor, p57^{Kip2}, exhibit skeletal abnormalities and growth retardation. J. Biochem. **127:**73–83.
34. **Tronche, F., et al.** 1999. Disruption of the glucocorticoid receptor gene in the nervous system results in reduced anxiety. Nat. Genet. **23:**99–103.

35. **Wechsler-Reya, R. J., and M. P. Scott.** 1999. Control of neuronal precursor proliferation in the cerebellum by sonic hedgehog. Neuron **22:**103–114.
36. **Weisheit, G., et al.** 2006. Postnatal development of the murine cerebellar cortex: formation and early dispersal of basket, stellate and Golgi neurons. Eur. J. Neurosci. **24:**466–478.
37. **Yamasaki, L., et al.** 1996. Tumor induction and tissue atrophy in mice lacking E2F-1. Cell **85:**537–548.
38. **Yan, Y., J. Frisen, M. H. Lee, J. Massague, and M. Barbacid.** 1997. Ablation of the CDK inhibitor $p57^{Kip2}$ results in increased apoptosis and delayed differentiation during mouse development. Genes Dev. **11:**973–983.
39. **Ye, W., G. Mairet-Coello, E. Pasoreck, and E. Dicicco-Bloom.** 2009. Patterns of $p57^{Kip2}$ expression in embryonic rat brain suggest roles in progenitor cell cycle exit and neuronal differentiation. Dev. Neurobiol. **69:**1–21.
40. **Zhang, P., et al.** 1997. Altered cell differentiation and proliferation in mice lacking $p57^{KIP2}$ indicates a role in Beckwith-Wiedemann syndrome. Nature **387:**151–158.